

PC-Conv: Unifying Homophily and Heterophily with Two-fold Filtering

Bingheng Li,¹ Erlin Pan,¹ Zhao Kang^{1*}

¹ University of Electronic Science and Technology of China, Chengdu, Sichuan, China
 {bingheng86,wujisixsix6}@gmail.com, zkang@uestc.edu.cn

Abstract

Recently, many carefully crafted graph representation learning methods have achieved impressive performance on either strong heterophilic or homophilic graphs, but not both. Therefore, they are incapable of generalizing well across real-world graphs with different levels of homophily. This is attributed to their neglect of homophily in heterophilic graphs, and vice versa. In this paper, we propose a two-fold filtering mechanism to extract homophily in heterophilic graphs and vice versa. In particular, we extend the graph heat equation to perform heterophilic aggregation of global information from a long distance. The resultant filter can be exactly approximated by the Possion-Charlier (PC) polynomials. To further exploit information at multiple orders, we introduce a powerful graph convolution PC-Conv and its instantiation PCNet for the node classification task. Compared with state-of-the-art GNNs, PCNet shows competitive performance on well-known homophilic and heterophilic graphs. Our implementation is available at <https://github.com/uestclbh/PC-Conv>.

Introduction

Developing methods to handle graph data has received increasing attention in the past decade. Graph neural networks (GNNs), which jointly leverage topological structure and node attribute information, have achieved immense success on numerous graph-related learning tasks. For each node, GNNs recursively aggregate and transform attributes from its neighbors. Due to this information aggregation mechanism, strong homophily of the graph is an implicit condition for GNNs to achieve good performance in downstream tasks (McPherson, Smith-Lovin, and Cook 2001). Basically, homophily means that similar nodes are prone to connect to each other. As a pioneering GNNs architecture, GCN (Welling and Kipf 2016) and its variants (Wu et al. 2019; Klicpera, Bojchevski, and Günnemann 2019) all adopt a low-pass filter to achieve feature smoothing through information aggregation between neighboring nodes. We refer to these models as homophilic GNNs.

Some recent works point out that GNNs are subject to substantial performance degradation on heterophilic graphs, where connected nodes tend to have different labels (Pei

et al. 2020; Abu-El-Haija et al. 2019). To handle heterophilic data, many researchers try to modify the original GNN or even design new architectures and techniques (Zhu et al. 2020; Yan et al. 2022; Luan et al. 2022a, 2021; Li et al. 2022; Mao et al. 2023; Pan and Kang 2023)

Despite respectable results in heterophilic graphs, many heterophilic GNNs still struggle to maintain superiority on homophilic graphs. The over-exploitation of heterophilic nodes and carefully crafted designs often limit their performance on homophilic graphs. In fact, homophilic and heterophilic graphs are not independent of each other, and real graphs cannot easily be classified as homophilic or heterophilic. This is because the degree of heterophily is just a statistical concept that measures the percentage of connected nodes from different classes. For example, in popular heterophilic datasets like Actor, Cornell, and Penn94, more than 20% of connected nodes belong to the same class (Li et al. 2022). This phenomenon is even more pronounced on large datasets (Lim et al. 2021). Therefore, homophilic and heterophilic graphs should not be treated separately, and some graph-agnostic processing methods are desired. In particular, the homophily in heterophilic graphs should be deliberately explored, and vice versa. Thus, this boils down to two questions:

Q1: how to deliberately design the information aggregation mechanism for homophilic and heterophilic nodes?

Q2: how to design a plausible strategy to combine them?

In response to the first question, we analyze information aggregation from a local and global perspective. For homophilic nodes, the local topology helps to aggregate the neighbors and preserve the local feature information to some extent (Zhang et al. 2021). This operation can be achieved by a simple low-pass filter. For heterophilic nodes, in contrast, the local topology could diversify the characteristics of the nodes, deviating abnormally from the original features and making the nodes difficult to distinguish in downstream tasks (Zhu et al. 2020). Some methods enlarge the node neighborhood to alleviate this problem. However, the size of the neighborhood is hard to set and varies from node to node. Therefore, we propose to use the global structure information of heterophilic nodes for information aggregation. Unlike the complex model in (Li et al. 2022), we gener-

*Corresponding author

Copyright © 2024, Association for the Advancement of Artificial Intelligence (www.aaai.org). All rights reserved.

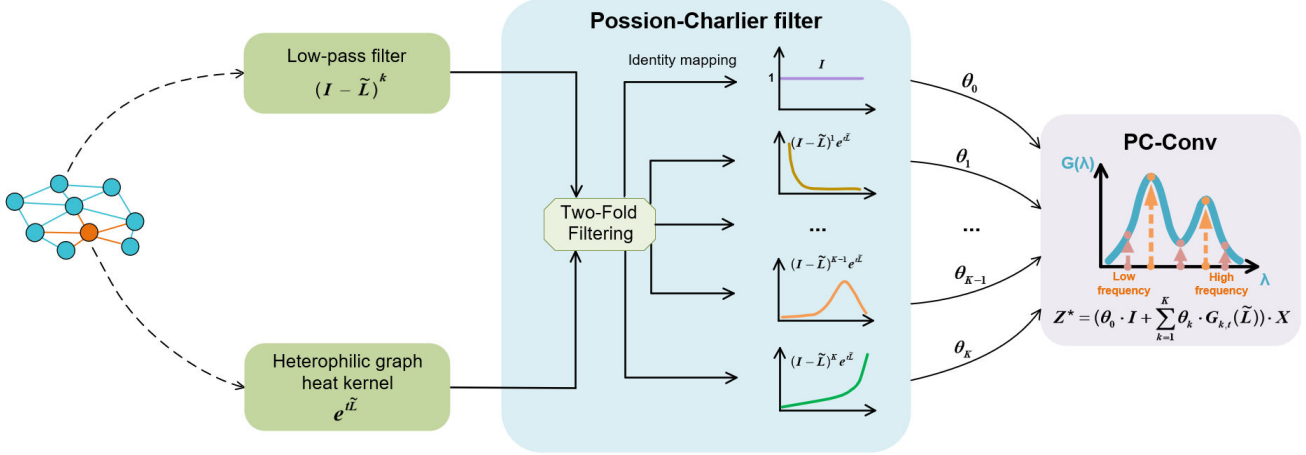


Figure 1: An illustration of our proposed PC-Conv.

alize the graph heat equation (Klicpera, Weißenberger, and Günnemann 2019; Xu et al. 2019) to the heterophilic graph and precompute the heterophilic heat kernel for global information aggregation.

For the second question, we propose a novel approach to combine filters based on our optimization framework: a two-fold filtering mechanism. Specifically, we integrate the heterophilic graph heat kernel with a local low-pass filter through two-fold filtering to yield a novel graph filter. To simplify its computation, we approximate it in an exact way with Possion-Charlier (PC) polynomials, dubbed as PC-filter.

In addition, to capture multi-order information, we propose to use PC-filter banks with adaptive coefficients, dubbed as PC-Conv, which is shown in Fig. 1. An exhaustive spectral analysis of PC-Conv is provided, including numerical approximation capability and flexibility in learning complex filters. Finally, a simple network architecture for node classification instantiates PC-Conv, i.e., PCNet, demonstrating the most advanced performance on both homophilic and heterophilic graphs. The main contributions of this paper are summarized as follows:

- **Two-fold filtering mechanism:** We develop a filtering strategy to perform both homophilic and heterophilic aggregation in any graph with different levels of homophily.
- **Heterophilic graph heat kernel:** We extend the graph heat kernel to heterophilic graph and integrate it with a low-pass filter to form a novel PC-filter.
- **PC-Conv:** We propose PC-Conv to explore multi-order information with learnable parameters. An exhaustive spectral analysis is also presented.
- **PCNet:** We instantiate PC-Conv with a simple GNN architecture, that is, PCNet. Experiments on node classification demonstrate the state-of-the-art (SOTA) performance.

Preliminaries

Notations. Define an undirected graph $\mathcal{G} = (\mathcal{V}, \mathcal{E})$ with a finite node set $|\mathcal{V}| = m$ and an edge set \mathcal{E} with $|\mathcal{E}|$ edges. We denote $i \sim j$ if node i and j are adjacent, otherwise $i \not\sim j$. Let $A \in \mathbb{R}^{m \times m}$ be the adjacency matrix, $A_{ij} = \begin{cases} 1, & i \sim j \\ 0, & i \not\sim j \end{cases}$, whose degree matrix D is diagonal with $D_{ii} = \sum_j A_{ij}$. Thus, the symmetric normalized adjacency matrix is $\tilde{A} = (D + I)^{-\frac{1}{2}}(A + I)(D + I)^{-\frac{1}{2}}$ and the normalized Laplacian matrix is $L = I - \tilde{A}$. We denote the node feature matrix by $X \in \mathbb{R}^{m \times d}$, where d is the dimensionality of the attribute. We use X_i and $X_{:j}$ to denote the feature vector of node i and the j -th graph signal, respectively.

Spectral Graph Convolution

Spectral graph convolution is the core of spectral GNNs (Bianchi et al. 2021) and can be unified as follows:

$$Z = g(L) \cdot X, \quad (1)$$

where Z is the output representation matrix. The key to the spectral graph convolution is the design of graph filter g . For Laplacian matrix $L = U\Lambda U^\top$, the eigenvalue matrix $\Lambda = \text{diag}(\lambda_1, \dots, \lambda_m)$ represents the frequency of the graph signal and $U = \{u_1, \dots, u_m\}$ is the frequency component associated with Λ . Given a graph signal x on \mathcal{G} , the graph Fourier transform and the inverse transform are defined as $\hat{x} = U^\top x$ and $x = U\hat{x}$, respectively. The purpose of designing a filter $g(L)$ is to adjust the frequency response of the graph signal. The graph convolution in the spectral domain can be expressed as:

$$z = g(L) \cdot x = U \cdot g(\Lambda) \cdot U^\top x = U \cdot g(\Lambda) \cdot \hat{x}. \quad (2)$$

Graph Heat Equation

(Weber 2010) defines the diffusion on the graph to characterize the global information flow, where the graph heat equation is proposed to depict the changes in node features during this process (Kloster and Gleich 2014). The graph heat

equation is generally written as:

$$\frac{dx(t)}{dt} = -Lx(t) \quad x(0) = x_0, \quad (3)$$

where $x(t)$ represents the feature information (graph signal) at time t . The solution is the heat kernel $x(t) = e^{-tL}x_0$. (Wang et al. 2021) uses the Euler method to approximate the heat kernel. Despite these methods have achieved decent results on homophilic graphs, their current form hinders their applications on heterophilic graphs.

Graph Optimization Framework

A classic graph optimization problem is (He et al. 2021):

$$\min_Z f(Z) = \text{Tr}(Z^\top h(L)Z) + \alpha \|Z - X\|_F^2, \quad (4)$$

where the first term is the smoothness constraint on the signals based on graph topological structure (Fu, Zhao, and Bian 2022) and $h(\cdot)$ servers as an energy function (Zhu et al. 2021). The second term enforces that Z retains as much information as possible from the original feature, where $\alpha > 0$ is a balance parameter. Problem (4) has a closed-form solution by setting $\frac{\partial f(Z)}{\partial Z} = 0$:

$$Z = g(L)X = (\alpha I + h(L))^{-1}X. \quad (5)$$

where $h(L)$ has to be positive semi-definite. If $h(L)$ is not positive semi-definite, then the optimization function $f(Z)$ is not convex, and the solution to $\frac{\partial f(Z)}{\partial Z} = 0$ may correspond to a saddle point. In terms of Eq.(5), we can establish the connection between $h(\cdot)$ and $g(\cdot)$, i.e.,

$$h(L) = g(L)^{-1} - \alpha I. \quad (6)$$

Therefore, different filters $g(L)$ correspond to different energy functions $h(L)$.

Methodology

Two-fold Filtering

The operation of the spectral filter on the feature matrix is equivalent to the information aggregation in the spatial domain (Balciar et al. 2021). From the spatial point of view, the low-pass filter makes the connected node features smooth and converge gradually; the high-pass filter sharpens the nodal features, making them easily distinguishable. The low-pass and high-pass filters correspond to two opposite ways of aggregating information in the spatial domain, which we refer them as homophilic aggregation and heterophilic aggregation, respectively. For a real graph with different levels of homophily, a single aggregation results in information loss. Therefore, we propose a two-fold filtering mechanism that performs homophilic and heterophilic aggregation of node features, which can be deduced from graph optimization.

heterophilic aggregation:

$$Y^* = \arg \min_Y \text{Tr}(Y^\top h_1(L)Y) + \alpha_1 \|Y - X\|_F^2 \quad (7)$$

homophilic aggregation:

$$Z^* = \arg \min_Z \text{Tr}(Z^\top h_2(L)Z) + \alpha_2 \|Z - Y^*\|_F^2 \quad (8)$$

where $h_1(L)$, $h_2(L)$ represent the energy function of heterophilic aggregation and homophilic aggregation, respectively. We can obtain the optimal solution from Eqs. (7-8):

$$Z^* = [(\alpha_1 I + h_1(L))(\alpha_2 I + h_2(L))]^{-1} X \quad (9)$$

Property 1. Z^* is order-invariant if we exchange the heterophilic and homophilic aggregation operations. (Proof in Appendix)

From another perspective, heterophilic and homophilic aggregation are conducted simultaneously. In the spatial domain, two-fold filtering can be seen as pushing nodes' features away from their neighbors to make some heterophilic nodes easily distinguishable and smoothing homophilic nodes with low-order information at the same time.

Heterophilic Graph Heat Kernel

To address the global information aggregation challenge for heterophilic nodes, we consider it from the perspective of graph diffusion. Eq. (3) mainly integrates global information in a homophilic graph. For heterophilic nodes, the complementary graph can provide missing-half structure, which can somehow mitigate inter-class information aggregation and enrich its structural information abundantly (Luan et al. 2019; Liu et al. 2021; Luan et al. 2022b; Zheng et al. 2023). We define a complementary graph \tilde{G} whose adjacency matrix $\tilde{A} = pI - A$, where p is a hyperparameter to measure the self-loop information. Denote $\tilde{L} = (p-2)I + L$, we can obtain the heterophilic propagation as $H_{hete} = e^{t\tilde{L}}X$. Based on Taylor expansion, we can formulate the information diffusion of the heterophilic graph as:

$$H_{hete} = \sum_{r=0}^{\infty} \frac{(t(p-1)I - A)^{2r+1}}{(2r+1)!} + \frac{(A - t(p-1)I)^{2r}}{(2r)!}.$$

We can see that the heterophilic graph heat kernel pushes the odd-order neighbors away and aggregates the neighborhood information for even-order neighbors, which is consistent with the structural property of the heterophilic graph. Different from existing works that only exploit even-order neighbors (Lei et al. 2022), our different treatments of odd-order and even-order neighbors allow us to dig for more holistic information. Furthermore, the heterophilic graph heat kernel can make use of infinite order information decaying with increasing order, which is also more flexible than (Welling and Kipf 2016; Velickovic et al. 2018; Hamilton, Ying, and Leskovec 2017) that fix the neighborhood size.

PC-Conv

For heterophilic aggregation, $g_1(\tilde{L}) = e^{t\tilde{L}}$ and the corresponding energy function is $h_1(\tilde{L}) = e^{-t\tilde{L}} - \alpha_1 I$. For homophilic aggregation, we use a low-pass filter to capture local low-order information and set $h_2(\tilde{L})$ to \tilde{L} for simplicity.

According to the requirements indicated in Preliminaries, $h_1(\tilde{L})$ in heterophilic aggregation and $h_2(\tilde{L})$ in homophilic aggregation need to be positive semi-definite, equivalently

constraining all eigenvalues of $h_1(\tilde{L})$ and $h_2(\tilde{L})$ to be non-negative, i.e.,

$$\begin{cases} h_1(\lambda) = \exp(-t(p-2+\lambda)) - \alpha_1 \geq 0, \forall \lambda \in [0, 2] \\ h_2(\lambda) = p-2+\lambda \geq 0, \forall \lambda \in [0, 2] \end{cases} \quad (10)$$

By solving the inequality above, we obtain the self-loop information measurement $p \in [2, -\frac{1}{t} \ln \alpha_1]$. For homophilic aggregation, $h_2(\tilde{L}) = \tilde{L}$ corresponds to a low-pass filter of $g_2(\tilde{L}) = (I + \alpha_2 \tilde{L})^{-1}$. To avoid matrix inversion, we use the first-order approximation as in the GCN (Welling and Kipf 2016). Generally, k -th order graph filtering can be written as $g_2(\tilde{L}) = (I - \alpha_2 \tilde{L})^k$, where k is a non-negative integer and is related to the degree of smoothing. For simplicity, we set $\alpha_2 = 1$ in our model. We have

$$Z^* = g_{k,t}(\tilde{L})X = (I - \tilde{L})^k e^{t\tilde{L}}X = U \cdot (I - \tilde{\lambda})^k e^{t\tilde{\lambda}} \cdot U^\top X. \quad (11)$$

In fact, BernNet (He et al. 2021) and JacobiConv (Wang and Zhang 2022) can also be viewed as a combination of local low-pass and local high-pass under two-fold filtering mechanism, i.e., $g(L) = \sum_{a,b}^K C_{ab} (2-L)^a L^b$, where C_{ab} is learnable coefficients with specific initialization. They can be decoupled into homophilic aggregation $(2I - L)^a$ and heterophilic aggregation L^b . Their heterophilic aggregation part is only localized, which may result in the neglect of global homophilic information (Li et al. 2022; Fang et al. 2022; Xie et al. 2023). By contrast, the heterophilic aggregation of PC-Conv is improved to $e^{t\tilde{L}}$, which utilizes the global information in a simple way while also strengthening the importance of even-order neighbors for heterophilic node (Lei et al. 2022).

In view of the exponential form of our spectral graph convolution, we use the Poisson-Charlier polynomial (Kroeker 1977) to make an exact numerical approximation.

Theorem 1. (Truesdell 1947) *The Poisson-Charlier polynomial is the coefficient of the power series expansion of the function $G(\gamma, t, \tilde{\lambda}) = (1 - \tilde{\lambda})^\gamma e^{t\tilde{\lambda}}$ by $\tilde{\lambda}$, i.e.,*

$$G(\gamma, t, \tilde{\lambda}) = \sum_{n=0}^{\infty} \frac{(-\tilde{\lambda})^n}{n!} C_n(\gamma, t) \quad \gamma, t \in \mathbb{R}, t > 0, \quad (12)$$

where $C_n(\gamma, t) = \sum_{k=0}^n C_n^k (-t)^k \gamma \cdots (\gamma - n + k + 1)$ is the Poisson-Charlier polynomial and it has the following recurrence relations:

$$\begin{aligned} C_0(\gamma, t) &= 1, C_1(\gamma, t) = \gamma - t, \dots, C_n(\gamma, t) = (\gamma - n - t + 1) \\ C_{n-1}(\gamma, t) - (n-1)t C_{n-2}(\gamma, t), n \geq 2 \end{aligned} \quad (13)$$

Corollary 1. Let $P_{\gamma,t}(\tilde{\lambda}) = \sum_{n=0}^N \frac{(-\tilde{\lambda})^n}{n!} C_n(\gamma, t)$ denote the Poisson-Charlier approximation of $G(\gamma, t, \tilde{\lambda})$. We have $P_{\gamma,t}(\tilde{\lambda}) \rightarrow G(\gamma, t, \tilde{\lambda})$ as $N \rightarrow \infty$.

Using the above approximation, we can obtain our PC-filter as :

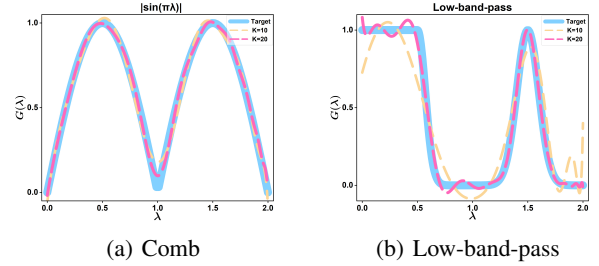


Figure 2: Illustrations of two complex filters and their approximations learned by PC-Conv.

$$\begin{aligned} g_{k,t}(\tilde{\lambda}) &= \sum_{n=0}^N \frac{(-\tilde{\lambda})^n}{n!} C_n(k, t), k \in \mathbb{Z}_+, \\ g_{k,t}(\tilde{\lambda}) &\rightarrow (I - \tilde{\lambda})^k e^{t\tilde{\lambda}}, N \rightarrow \infty. \end{aligned} \quad (14)$$

Using a single k for all nodes means that the degree of local information aggregation is fixed, which would lead to an under-smoothing problem (Zhang et al. 2021; Pan and Kang 2021). To make full use of node features at multiple orders, we introduce a learnable parameter θ_k to aggregate node information from k -order neighbors, where each term can be considered as a single layer filter.

In addition, for graphs with a high degree of heterophily, topology structure-based aggregation may not learn a good representation. Motivated by (Chen et al. 2020), we use identity mapping to incorporate raw node features and ensure that the representation can at least achieve the same performance as the original data. Finally, we formulate our Possion-Charlier convolution (PC-Conv) as:

$$\begin{aligned} Z^* &= g_t(\tilde{L})X = U(\theta_0 + \sum_{k=1}^K \theta_k \cdot g_{k,t}(\tilde{\lambda}))U^\top X \\ &= \theta_0 \cdot X + \sum_{k=1}^K \theta_k \cdot \sum_{n=0}^N C_n(k, t) \frac{(-\tilde{\lambda})^n}{n!} X \end{aligned} \quad (15)$$

where $C_n(k, t)$ is computed through Eq. (13).

Spectral Analysis

Assuming there exists a perfect filter function $G(\lambda)$ that can best match the downstream task, the objective of filter learning is to approximate $G(\lambda)$ as accurately as possible.

Theorem 2. *When $N \geq K$, $t \notin \{1, 2, \dots, K\}$, any N order differentiable real value filter function can be approximated by N -order PC-Conv, with an error of order $N+1$. (Proof in Appendix)*

Corollary 2. *PC-Conv can learn arbitrary polynomial filters with order up to N , where $N \geq K$, $t \notin \{1, 2, \dots, K\}$.*

Therefore, PC-Conv belongs to *Polynomial-Filter-Most-Expressive* (PFME) Convolution (Wang and Zhang 2022), whose learning ability is positively correlated with K . Since the eigenvalues of graph Laplacian matrix are discrete and can be interpolated precisely by polynomials, PC-Conv can

Table 1: The computational complexity of relevant polynomial-based methods.

Model	Computational Complexity
MLP	$O(mFd + mdC)$
GPRGNN	$O(K E C) + O(mKC)$
BernNet	$O(K^2 E C) + O(mKC) + O(K)$
JacobiConv	$O(K E C) + O(mKC) + O(K)$
ChebNetII	$O(K E C) + O(mKC) + O(K)$
PC-Conv	$O(N E C) + O(mNKC) + O(N)$

be further classified as *Filter-Most-Expressive* (FME) Convolution, which can express arbitrary real-valued filter functions.

Accordingly, PC-Conv can learn more complex filters than low-pass and high-pass filters, such as comb and band-pass filters. In Fig. 2, we plot two difficult filters that are learned by PC-Conv in an end-to-end fashion. The low-band-pass filter is $G(\lambda) = I_{[0,0.5]}(\lambda) + \exp(-100(\lambda - 0.5)^2)I_{(0.5,1)}(\lambda) + \exp(-50(\lambda - 1.5)^2)I_{[1,2]}(\lambda)$, where $I_{\Omega}(\lambda) = 1$ when $\lambda \in \Omega$, otherwise $I_{\Omega}(\lambda) = 0$ (He et al. 2021). We can observe that PC-Conv learns well and the approximation accuracy increases with K , which is in line with the above theory.

PCNet for Node Classification

Based on PC-Conv, we propose PCNet architecture for the node classification task, which contains three components: generalized normalization of the graph Laplacian matrix, the computation of PC-Conv, and the classification module.

(Jin et al. 2022) analyzes the overcorrelation issue in spectral GNNs. (Yang et al. 2022) points out that the fixed range $[-1, 1]$ of standard Laplacian normalization is not a good choice due to the diminishing problem. Generalized normalization can alleviate this problem by shrinking the spectrum (Zhang et al. 2022). Thus, we introduce the hyperparameter η into PCNet.

$$\tilde{A} = (D + I)^{-\eta}(A + I)(D + I)^{-\eta} \quad (16)$$

Then, our Laplacian matrix \tilde{L} becomes:

$$\tilde{L} = (p - 1)I - (D + I)^{-\eta}(A + I)(D + I)^{-\eta} \quad (17)$$

Then, we calculate the Poisson-Charlie polynomial according to Eq. (13). Different from existing works, PC polynomial serves as coefficients in our convolution. Therefore, the time complexity of this process is $O(N)$. The construction of PC-Conv can be seen as two processes. The first step is to calculate the generalized Laplacian matrix for message transmission, i.e., $\tilde{L}^i \Theta(X)$, $i \in 0, \dots, N$, where $\Theta(X) \in R^{m \times C}$ is the transformed feature matrix for C classes, usually an MLP or linear layer. The time complexity is $O(N|E|C)$. The second step is to combine it with PC coefficients according to Eq. (14), whose time complexity is $O(mNKC)$. The total computational complexity of our PC-Conv is $O(N|E|C) + O(mNKC) + O(N)$. The first

term dominates the others in practice. We list the computational complexity of relevant methods in Table 1. Compared to $O(K|E|C)$ in other methods with $K = 10$, PC-Conv is more efficient since N is often smaller than K . Therefore, our method doesn't incur extra computation burden w.r.t. other SOTA methods. The node classification with PCNet is:

$$Z^* = \text{softmax} \left((\theta_0 + \sum_{k=1}^K \theta_k \cdot g_{k,t}(\tilde{\lambda})) \Theta(X) \right), \quad (18)$$

$$\mathcal{L} = - \sum_{l \in \mathcal{Y}_L} \sum_{c=1}^C Y_{lc} \ln Z_{lc}^*,$$

where \mathcal{Y}_L is the labeled node indices and the cross-entropy loss over label matrix Y is applied to train the GCN network. The coefficient θ_k is updated by the backward propagation of the loss.

Experiment

Dataset

For the sake of fairness, we select benchmark datasets that are commonly used in related work. For the homophilic graph, we select three classic citation graphs: Cora, CiteSeer, PubMed (Yang, Cohen, and Salakhudinov 2016). For the heterophilic graph, we select four datasets including the Webpage graphs Texas, Cornell, and Wisconsin from WebKB3¹, and the Actor co-occurrence graph (Pei et al. 2020). Besides, we also select Penn94 from Facebook 100² as a representative dataset of the social network (Lim et al. 2021).

Train/validation/test split

For semi-supervised node classification, we split the dataset with random seeds according to (He, Wei, and Wen 2022). In detail, we select 20 nodes of each class on three homophilic datasets (Cora, Citeser, and Pubmed) for training, 500 nodes for validation, and 1000 nodes for testing. For the three heterophilic datasets (Texas, Actor, Cornell), we apply the sparse splitting where the training/validation/test sets account for 2.5%/2.5%/95%.

For node classification, there are two common split ways: random seed splits and fixed seed splits. The former, proposed by (Chien et al. 2021), uses random seeds for random split and is widely used in spectral GNNs, PDE GNNs, traditional methods, etc. The latter uses the fixed split given in (Li et al. 2022), which is commonly used in heterophilic GNNs. To avoid unfair comparison, we evaluate the performance of PCNet under these two different settings. For the node classification with polynomial-based methods, we adopt 10 random seeds as (Chien et al. 2021; Wang and Zhang 2022) to randomly split the dataset into train/validation/test sets with a ratio of 60%/20%/20%. For node classification with heterophilic GNNs, we use the given split in (Li et al. 2022) to randomly split the dataset into training/validation/test sets at a ratio of 48%/32%/20%.

¹<http://www.cs.cmu.edu/afs/cs.cmu.edu/project/theo-11/www/wwkb>

²<https://archive.org/details/oxford-2005-facebook-matrix>

Table 2: The results of semi-supervised node classification: Mean accuracy (%) \pm 95% confidence interval. We highlight the best score in red and the runner-up score with blue.

Dataset	MLP	GCN	ChebNet	ARMA	APPNP	GPRGNN	BernNet	ChebNetII	PCNet
Cora	57.17 \pm 1.34	79.19 \pm 1.37	78.08 \pm 0.86	79.14 \pm 1.07	82.39 \pm 0.68	82.37 \pm 0.91	82.17 \pm 0.86	82.42 \pm 0.64	82.81 \pm 0.50
CiteSeer	56.75 \pm 1.55	69.71 \pm 1.32	67.87 \pm 1.49	69.35 \pm 1.44	69.79 \pm 0.92	69.22 \pm 1.27	69.44 \pm 0.97	69.89 \pm 1.21	69.92 \pm 0.70
PubMed	70.52 \pm 0.27	78.81 \pm 0.24	73.96 \pm 0.31	78.31 \pm 0.22	79.97 \pm 0.28	79.28 \pm 0.33	79.48 \pm 0.41	79.51 \pm 1.03	80.01 \pm 0.88
Texas	32.42 \pm 9.91	34.68 \pm 9.07	36.35 \pm 8.90	39.65 \pm 8.09	34.79 \pm 10.11	33.98 \pm 11.90	43.01 \pm 7.45	46.58 \pm 7.68	64.56 \pm 1.84
Actor	29.75 \pm 0.95	22.74 \pm 2.37	26.58 \pm 1.92	27.02 \pm 2.31	29.74 \pm 1.04	28.58 \pm 1.01	29.87 \pm 0.78	30.18 \pm 0.81	33.56 \pm 0.40
Cornell	36.53 \pm 7.92	32.36 \pm 8.55	28.78 \pm 4.85	28.90 \pm 10.07	34.85 \pm 9.71	38.95 \pm 12.36	39.42 \pm 9.59	42.19 \pm 11.61	52.08 \pm 4.45

Table 3: Mean accuracy (%) of node classification with polynomial-based methods.

Method	Cora	Citeseir	Pubmed	Texas	Actor	Cornell
MLP	76.89 \pm 0.97	76.52 \pm 0.89	86.14 \pm 0.25	86.81 \pm 2.24	40.18 \pm 0.55	84.15 \pm 3.05
GCN	87.18 \pm 1.12	79.85 \pm 0.78	86.79 \pm 0.31	76.97 \pm 3.97	33.26 \pm 1.15	65.78 \pm 4.16
ChebNet	87.32 \pm 0.92	79.33 \pm 0.57	87.82 \pm 0.24	86.28 \pm 2.62	37.42 \pm 0.58	83.91 \pm 2.17
ARMA	87.13 \pm 0.80	80.04 \pm 0.55	86.93 \pm 0.24	83.97 \pm 3.77	37.67 \pm 0.54	85.62 \pm 2.13
APPNP	88.16 \pm 0.74	80.47 \pm 0.73	88.13 \pm 0.33	90.64 \pm 1.70	39.76 \pm 0.49	91.52 \pm 1.81
GCNII	88.46 \pm 0.82	79.97 \pm 0.65	89.94 \pm 0.31	80.46 \pm 5.91	36.89 \pm 0.95	84.26 \pm 2.13
TWIRLS	88.57 \pm 0.91	80.07 \pm 0.94	88.87 \pm 0.43	91.31 \pm 3.36	38.13 \pm 0.81	89.83 \pm 2.29
EGNN	87.47 \pm 1.33	80.51 \pm 0.93	88.74 \pm 0.46	81.34 \pm 1.56	35.16 \pm 0.64	82.09 \pm 1.16
PDE-GCN	88.62 \pm 1.03	79.98 \pm 0.97	89.92 \pm 0.38	93.24 \pm 2.03	39.76 \pm 0.74	89.73 \pm 1.35
GPRGNN	88.54 \pm 0.67	80.13 \pm 0.84	88.46 \pm 0.31	92.91 \pm 1.32	39.91 \pm 0.62	91.57 \pm 1.96
BernNet	88.51 \pm 0.92	80.08 \pm 0.75	88.51 \pm 0.39	92.62 \pm 1.37	41.71 \pm 1.12	92.13 \pm 1.64
EvenNet	87.25 \pm 1.42	78.65 \pm 0.96	89.52 \pm 0.31	93.77 \pm 1.73	40.48 \pm 0.62	92.13 \pm 1.72
ChebNetII	88.71 \pm 0.93	80.53 \pm 0.79	88.93 \pm 0.29	93.28 \pm 1.47	41.75 \pm 1.07	92.30 \pm 1.48
JacobiConv	88.98 \pm 0.46	80.78 \pm 0.79	89.62 \pm 0.41	93.44 \pm 2.13	41.17 \pm 0.64	92.95 \pm 2.46
PCNet	90.02 \pm 0.62	81.76 \pm 0.78	91.30 \pm 0.38	95.57 \pm 1.31	42.72 \pm 0.91	93.83 \pm 1.91

Semi-supervised Node Classification

Settings: We compare the performance of PCNet with eight polynomial approximation methods of spectral filtering, including MLP, GCN (Welling and Kipf 2016), APPNP (Klicpera, Bojchevski, and Günnemann 2019), ChebNet (Defferrard, Bresson, and Vandergheynst 2016), ARMA (Bianchi et al. 2021), GPRGNN (Chien et al. 2021), BernNet (He et al. 2021), and ChebNetII (He, Wei, and Wen 2022). For PCNet, we use the same settings for all experiments. Specifically, we apply MLP to dimensionally process the features and set the hidden units to 64 for fairness (Chien et al. 2021; He, Wei, and Wen 2022). To reduce computation load, we set $K = 4 \sim 6$.

Result: We can observe that PCNet outperforms all other methods in Table 2. PCNet even achieves a performance improvement of 10% \sim 20% on two heterophilic datasets: Texas and Cornell. In fact, under sparse split, the performance of many methods fluctuates a lot with the choice of the training set. By contrast, the fluctuations in PCNet are small, which reflects the stability of PCNet. Furthermore, PCNet uses only 4 \sim 6 PC-filters, achieving competitive performance yet saving computational overhead.

Node Classification with Polynomial-based Methods

Settings: Besides JacobiConv (Wang and Zhang 2022) and EvenNet (Lei et al. 2022), we also include four competitive

baselines for node classification: GCNII (Chen et al. 2020), TWIRLS (Yang et al. 2021), EGNN (Zhou et al. 2021), and PDE-GCN (Eliasof, Haber, and Treister 2021), which make full use of the topology information from different perspectives including GNNs architecture, energy function, and PDE GNNs.

Result: Table 3 shows that PCNet achieves the best performance on all datasets and has at least 1% gain w.r.t. the second best performance. PCNet’s excellent performance on both homophilic and heterophilic graphs is due to our two-fold filtering which captures the co-existence of homophily and heterophily in real datasets. In addition, the heterophilic heat kernel also contributes to this superior performance by aggregating more distant (and even infinite-order) neighbor information compared to BernNet and JacobiConv.

Node Classification with Heterophilic GNNs

Settings: We add some heterophilic methods, including (1) Spatial heterophilic GNNs: H2GCN (Zhu et al. 2020), WR-GAT (Suresh et al. 2021), GloGNN++ (Li et al. 2022); (2) GNNs with filterbank: GPRGNN (Chien et al. 2021) and ACM-GCN (Luan et al. 2021); (3) MLP-based methods: LINKX (Lim et al. 2021); (4) Scalable heterophilic GNNs: GCNII (Chen et al. 2020) and GGCN (Yan et al. 2022).

Result: PCNet achieves the top average ranking on all datasets in Table 4. In particular, it outperforms recent heterophilic methods GloGNN++ and GGCN on 6 out of 8

Table 4: Mean accuracy (%) of node classification by the heterophilic methods. OOM refers to the out-of-memory error.

Dataset	Cora	Citeseer	Pubmed	Texas	Actor	Cornell	Wisconsin	Penn94	Avg. Rank
MLP	75.69 ± 2.00	74.02 ± 1.90	87.16 ± 0.37	80.81 ± 4.75	36.53 ± 0.70	81.89 ± 6.40	85.29 ± 3.31	73.61 ± 0.40	9.19
GCN	86.98 ± 1.27	76.50 ± 1.36	88.42 ± 0.50	55.14 ± 5.16	27.32 ± 1.10	60.54 ± 5.30	51.76 ± 3.06	82.47 ± 0.27	10.75
GAT	87.30 ± 1.10	76.55 ± 1.23	86.33 ± 0.48	52.16 ± 6.63	27.44 ± 0.89	61.89 ± 5.05	49.41 ± 4.09	81.53 ± 0.55	11.13
MixHop	87.61 ± 0.85	76.26 ± 1.33	85.31 ± 0.61	77.84 ± 7.73	32.22 ± 2.34	73.51 ± 6.34	75.88 ± 4.90	83.47 ± 0.71	9.75
GCNII	88.37 ± 1.25	77.33 ± 1.48	90.15 ± 0.43	77.57 ± 3.83	37.44 ± 1.30	77.86 ± 3.79	80.39 ± 3.40	82.92 ± 0.59	5.25
H ₂ GCN	87.87 ± 1.20	77.11 ± 1.57	89.49 ± 0.38	84.86 ± 7.23	35.70 ± 1.00	82.70 ± 5.28	87.65 ± 4.98	81.31 ± 0.60	6.19
WRGAT	88.20 ± 2.26	76.81 ± 1.89	88.52 ± 0.92	83.62 ± 5.50	36.53 ± 0.77	81.62 ± 3.90	86.98 ± 3.78	74.32 ± 0.53	6.69
GPRGNN	87.95 ± 1.18	77.13 ± 1.67	87.54 ± 0.38	78.38 ± 4.36	34.63 ± 1.22	80.27 ± 8.11	82.94 ± 4.21	81.38 ± 0.16	8.06
GGCN	87.95 ± 1.05	77.14 ± 1.45	89.15 ± 0.37	84.86 ± 4.55	37.54 ± 1.56	85.68 ± 6.63	86.86 ± 3.22	OOM	5.50
ACM-GCN	87.91 ± 0.95	77.32 ± 1.70	90.00 ± 0.52	87.84 ± 4.40	36.28 ± 1.09	85.14 ± 6.07	88.43 ± 3.22	82.52 ± 0.96	4.00
LINKX	84.64 ± 1.13	73.19 ± 0.99	87.86 ± 0.77	74.60 ± 8.37	36.10 ± 1.55	77.84 ± 5.81	75.49 ± 5.72	84.71 ± 0.52	9.63
GloGNN++	88.33 ± 1.09	77.22 ± 1.78	89.24 ± 0.39	84.05 ± 4.90	37.70 ± 1.40	85.95 ± 5.10	88.04 ± 3.22	85.74 ± 0.42	3.00
PCNet	88.41 ± 0.66	77.50 ± 1.06	89.51 ± 0.28	88.11 ± 2.17	37.80 ± 0.64	82.16 ± 2.70	88.63 ± 2.75	84.75 ± 0.51	1.88

Table 5: Results of ablation study on PC-Conv with MLP and single linear layer.

Datasets	Monomial	Chebyshev	Bernstein	Jacobi	PCNet _{0.5} -Lin		GPRGNN	ChebNet	BernNet	Jacobi-MLP	PCNet _{0.5}
Cora	88.80 ± 0.67	88.49 ± 0.82	86.50 ± 1.26	88.98 ± 0.72	90.04 ± 0.71		88.54 ± 0.67	87.32 ± 0.92	88.51 ± 0.92	88.67 ± 0.69	90.00 ± 0.49
Citeseer	80.68 ± 0.86	80.53 ± 0.81	80.61 ± 0.85	80.61 ± 0.72	81.17 ± 0.66		80.13 ± 0.84	79.33 ± 0.57	80.08 ± 0.75	80.25 ± 0.60	82.10 ± 0.72
Pubmed	89.54 ± 0.36	89.52 ± 0.46	88.42 ± 0.32	89.70 ± 0.34	90.97 ± 0.27		88.46 ± 0.31	87.82 ± 0.24	88.51 ± 0.92	87.73 ± 2.13	91.58 ± 0.95
Texas	91.64 ± 2.46	88.36 ± 3.93	89.34 ± 2.46	92.79 ± 1.97	95.25 ± 1.15		92.91 ± 1.32	87.82 ± 0.24	92.62 ± 1.37	89.34 ± 3.12	95.25 ± 0.82
Actor	40.31 ± 0.82	40.61 ± 0.64	40.42 ± 0.50	40.70 ± 0.98	39.56 ± 1.00		39.91 ± 0.62	37.42 ± 0.58	41.71 ± 1.12	37.56 ± 0.88	41.79 ± 0.70
Cornell	91.31 ± 2.13	88.03 ± 3.28	92.46 ± 2.63	92.30 ± 2.79	92.62 ± 1.97		91.57 ± 1.96	83.91 ± 2.17	92.13 ± 1.64	87.54 ± 3.11	92.32 ± 1.48

datasets. The superior performance is attributed to our two-fold filtering, which not only explores global information but also mines homophily in heterophilic graphs. Thus PCNet generalizes well to both homophilic and heterophilic graphs. We also see the importance of node features, which provide rich information different from heterophilic structure. Thus MLP can outperform GCN and GAT by more than 20% in Texas and Cornell. This validates the necessity of identity mapping.

Ablation Study on PC-Conv

To examine the contribution of generalized Laplacian normalization, we replace η with 0.5, i.e., we use traditional Laplacian. The classification results on six datasets are 82.33 ± 0.83 , 69.01 ± 1.08 , 79.73 ± 0.97 , 57.55 ± 2.66 , 33.28 ± 0.63 , 48.03 ± 7.69 . Though they outperform other methods in Table 2, they are still lower than that of PCNet. Thus, it is beneficial to introduce spectral scaling.

Furthermore, to test the effect of PC-Conv without relying on any trick (generalized Laplacian normalization), we compare popular polynomial bases (Monomial (Chien et al. 2021), Chebyshev (Defferrard, Bresson, and Vandergheynst 2016), Bernstein (He et al. 2021), Jacobi (Wang and Zhang 2022)) to demonstrate the superiority of PC-Conv. In order to exclude the effect of dimensional transformations, both MLP and individual linear layers are applied, and the corresponding models are denoted as PCNet_{0.5} and PCNet_{0.5}-LIN respectively. The results on node classification are shown in Table 5, from which we can see that PCNet_{0.5} and PCNet_{0.5}-LIN can still beat others in most cases. Moreover, the performance of PCNet_{0.5} and PCNet_{0.5}-LIN is close to

each other in 5 out of 6 datasets, indicating that PC-Conv is robust to the dimensional transformation.

Finally, we remove the identity mapping from PC-Conv, leaving the combinations of PC-filters. The classification performance on those six datasets are 89.92 ± 0.95 , 81.01 ± 0.63 , 90.96 ± 0.35 , 95.25 ± 2.30 , 42.11 ± 0.92 , 93.44 ± 2.13 . We can observe that the accuracy is inferior to that of PCNet in Table 2. But compared to other SOTA methods, they are still better, which illustrates the superiority of the PC-filter itself.

Conclusion

Motivated by the coexistence of homophilic and heterophilic nodes in real graphs, we propose a two-fold filtering mechanism to simultaneously perform homophilic and heterophilic information aggregation. For the first time, we extend the graph heat kernel to heterophilic graphs to exploit the global information. The proposed PC-filter makes full use of data information and PC-Conv performs adaptive graph convolution. The PCNet architecture for node classification achieves state-of-the-art performance on real-world datasets. One limitation is that our knowledge of homophily is limited, thus we just use the simplest low-pass filter, which deserves more attention in the future.

References

Abu-El-Haija, S.; Perozzi, B.; Kapoor, A.; Alipourfard, N.; Lerman, K.; Harutyunyan, H.; Ver Steeg, G.; and Galstyan, A. 2019. Mixhop: Higher-order graph convolutional architectures via sparsified neighborhood mixing. In *International Conference on Machine Learning*, 21–29. PMLR.

Balcilar, M.; Guillaume, R.; Héroux, P.; Gaižiūne, B.; Adam, S.; and Honeine, P. 2021. Analyzing the expressive power of graph neural networks in a spectral perspective. In *International Conference on Learning Representations*.

Bianchi, F. M.; Grattarola, D.; Livi, L.; and Alippi, C. 2021. Graph Neural Networks with convolutional ARMA filters. *IEEE Transactions on Pattern Analysis and Machine Intelligence*.

Chen, M.; Wei, Z.; Huang, Z.; Ding, B.; and Li, Y. 2020. Simple and deep graph convolutional networks. In *International Conference on Machine Learning*, 1725–1735. PMLR.

Chien, E.; Peng, J.; Li, P.; and Milenkovic, O. 2021. Adaptive Universal Generalized PageRank Graph Neural Network. In *International Conference on Learning Representations*.

Defferrard, M.; Bresson, X.; and Vandergheynst, P. 2016. Convolutional Neural Networks on Graphs with Fast Localized Spectral Filtering. In *Advances in Neural Information Processing Systems*, 3837–3845.

Eliasof, M.; Haber, E.; and Treister, E. 2021. Pde-gcn: Novel architectures for graph neural networks motivated by partial differential equations. *Advances in Neural Information Processing Systems*, 34: 3836–3849.

Fang, R.; Wen, L.; Kang, Z.; and Liu, J. 2022. Structure-preserving graph representation learning. In *2022 IEEE International Conference on Data Mining (ICDM)*, 927–932. IEEE.

Fu, G.; Zhao, P.; and Bian, Y. 2022. p -Laplacian Based Graph Neural Networks. In *International Conference on Machine Learning*, 6878–6917. PMLR.

Hamilton, W.; Ying, Z.; and Leskovec, J. 2017. Inductive representation learning on large graphs. *Advances in Neural Information Processing Systems*, 30.

He, M.; Wei, Z.; and Wen, J. 2022. Convolutional Neural Networks on Graphs with Chebyshev Approximation, Revisited. *Advances in Neural Information Processing Systems*.

He, M.; Wei, Z.; Xu, H.; et al. 2021. Bernnet: Learning arbitrary graph spectral filters via bernstein approximation. *Advances in Neural Information Processing Systems*, 34: 14239–14251.

Jin, W.; Liu, X.; Ma, Y.; Aggarwal, C.; and Tang, J. 2022. Feature Overcorrelation in Deep Graph Neural Networks: A New Perspective. In *Proceedings of the ACM Conference on Knowledge Discovery and Data Mining (KDD)*, KDD ’22, 709–719. Association for Computing Machinery.

Klicpera, J.; Bojchevski, A.; and Günnemann, S. 2019. Predict then Propagate: Graph Neural Networks meet Personalized PageRank. In *International Conference on Learning Representations*.

Klicpera, J.; Weissenberger, S.; and Günnemann, S. 2019. Diffusion improves graph learning. *Advances in Neural Information Processing Systems*.

Kloster, K.; and Gleich, D. F. 2014. Heat kernel based community detection. In *Proceedings of the 20th ACM SIGKDD international conference on Knowledge discovery and data mining*, 1386–1395.

Kroeker, J. 1977. Wiener analysis of nonlinear systems using Poisson-Charlier crosscorrelation. *Biological Cybernetics*, 27(4): 221–227.

Lei, R.; Wang, Z.; Li, Y.; Ding, B.; and Wei, Z. 2022. Even-Net: Ignoring Odd-Hop Neighbors Improves Robustness of Graph Neural Networks. *Advances in Neural Information Processing Systems*.

Li, X.; Zhu, R.; Cheng, Y.; Shan, C.; Luo, S.; Li, D.; and Qian, W. 2022. Finding Global Homophily in Graph Neural Networks When Meeting Heterophily. In *International Conference on Machine Learning*. PMLR.

Lim, D.; Hohne, F.; Li, X.; Huang, S. L.; Gupta, V.; Bhalerao, O.; and Lim, S. N. 2021. Large scale learning on non-homophilous graphs: New benchmarks and strong simple methods. *Advances in Neural Information Processing Systems*, 34: 20887–20902.

Liu, C.; Wen, L.; Kang, Z.; Luo, G.; and Tian, L. 2021. Self-supervised consensus representation learning for attributed graph. In *Proceedings of the 29th ACM international conference on multimedia*, 2654–2662.

Luan, S.; Hua, C.; Lu, Q.; Zhu, J.; Zhao, M.; Zhang, S.; Chang, X.-W.; and Precup, D. 2021. Is Heterophily A Real Nightmare For Graph Neural Networks To Do Node Classification? *arXiv preprint arXiv:2109.05641*.

Luan, S.; Hua, C.; Lu, Q.; Zhu, J.; Zhao, M.; Zhang, S.; Chang, X.-W.; and Precup, D. 2022a. Revisiting heterophily for graph neural networks. *Advances in neural information processing systems*, 35: 1362–1375.

Luan, S.; Zhao, M.; Chang, X.-W.; and Precup, D. 2019. Break the ceiling: Stronger multi-scale deep graph convolutional networks. *Advances in neural information processing systems*, 32.

Luan, S.; Zhao, M.; Hua, C.; Chang, X.-W.; and Precup, D. 2022b. Complete the Missing Half: Augmenting Aggregation Filtering with Diversification for Graph Convolutional Networks. In *NeurIPS 2022 Workshop: New Frontiers in Graph Learning*.

Mao, H.; Chen, Z.; Jin, W.; Han, H.; Ma, Y.; Zhao, T.; Shah, N.; and Tang, J. 2023. Demystifying Structural Disparity in Graph Neural Networks: Can One Size Fit All? *Advances in neural information processing systems*.

McPherson, M.; Smith-Lovin, L.; and Cook, J. M. 2001. Birds of a feather: Homophily in social networks. *Annual review of sociology*, 415–444.

Pan, E.; and Kang, Z. 2021. Multi-view contrastive graph clustering. *Advances in neural information processing systems*, 34: 2148–2159.

Pan, E.; and Kang, Z. 2023. Beyond Homophily: Reconstructing Structure for Graph-agnostic Clustering. In *International Conference on Machine Learning*. PMLR.

Pei, H.; Wei, B.; Chang, K. C.-C.; Lei, Y.; and Yang, B. 2020. Geom-GCN: Geometric Graph Convolutional Networks. In *International Conference on Learning Representations*.

Suresh, S.; Budde, V.; Neville, J.; Li, P.; and Ma, J. 2021. Breaking the Limit of Graph Neural Networks by Improving the Assortativity of Graphs with Local Mixing Patterns. In *Proceedings of the 27th ACM SIGKDD Conference on Knowledge Discovery & Data Mining*.

Truesdell, C. 1947. A Note on the Poisson-Charlier Functions. *The Annals of Mathematical Statistics*, 18(3): 450–454.

Velickovic, P.; Cucurull, G.; Casanova, A.; Romero, A.; Liò, P.; and Bengio, Y. 2018. Graph Attention Networks. In *International Conference on Learning Representations*.

Wang, X.; and Zhang, M. 2022. How Powerful are Spectral Graph Neural Networks. In *International Conference on Machine Learning*, 23341–23362. PMLR.

Wang, Y.; Wang, Y.; Yang, J.; and Lin, Z. 2021. Dissecting the diffusion process in linear graph convolutional networks. *Advances in Neural Information Processing Systems*, 34: 5758–5769.

Weber, A. 2010. Analysis of the physical Laplacian and the heat flow on a locally finite graph. *Journal of Mathematical Analysis and Applications*, 1(370): 146–158.

Welling, M.; and Kipf, T. N. 2016. Semi-supervised classification with graph convolutional networks. In *J. International Conference on Learning Representations (ICLR 2017)*.

Wu, F.; Souza, A.; Zhang, T.; Fifty, C.; Yu, T.; and Weinberger, K. 2019. Simplifying graph convolutional networks. In *International Conference on Machine Learning*, 6861–6871. PMLR.

Xie, X.; Chen, W.; Kang, Z.; and Peng, C. 2023. Contrastive graph clustering with adaptive filter. *Expert Systems with Applications*, 219: 119645.

Xu, B.; Shen, H.; Cao, Q.; Cen, K.; and Cheng, X. 2019. Graph convolutional networks using heat kernel for semi-supervised learning. In *IJCAI*.

Yan, Y.; Hashemi, M.; Swersky, K.; Yang, Y.; and Koutra, D. 2022. Two Sides of the Same Coin: Heterophily and Oversmoothing in Graph Convolutional Neural Networks. In *2022 IEEE International Conference on Data Mining*. IEEE.

Yang, M.; Shen, Y.; Li, R.; Qi, H.; Zhang, Q.; and Yin, B. 2022. A new perspective on the effects of spectrum in graph neural networks. In *International Conference on Machine Learning*, 25261–25279. PMLR.

Yang, Y.; Liu, T.; Wang, Y.; Zhou, J.; Gan, Q.; Wei, Z.; Zhang, Z.; Huang, Z.; and Wipf, D. 2021. Graph neural networks inspired by classical iterative algorithms. In *International Conference on Machine Learning*, 11773–11783. PMLR.

Yang, Z.; Cohen, W.; and Salakhudinov, R. 2016. Revisiting semi-supervised learning with graph embeddings. In *International Conference on Machine Learning*, 40–48. PMLR.

Zhang, W.; Sheng, Z.; Yang, M.; Li, Y.; Shen, Y.; Yang, Z.; and Cui, B. 2022. NAFS: A Simple yet Tough-to-beat Baseline for Graph Representation Learning. In *Proceedings of the 39th International Conference on Machine Learning*, volume 162, 26467–26483. PMLR.

Zhang, W.; Yang, M.; Sheng, Z.; Li, Y.; Ouyang, W.; Tao, Y.; Yang, Z.; and Cui, B. 2021. Node dependent local smoothing for scalable graph learning. *Advances in Neural Information Processing Systems*, 34: 20321–20332.

Zheng, Y.; Zhang, H.; Lee, V.; Zheng, Y.; Wang, X.; and Pan, S. 2023. Finding the Missing-half: Graph Complementary Learning for Homophily-prone and Heterophily-prone Graphs. In *International Conference on Machine Learning*. PMLR.

Zhou, K.; Huang, X.; Zha, D.; Chen, R.; Li, L.; Choi, S.-H.; and Hu, X. 2021. Dirichlet energy constrained learning for deep graph neural networks. *Advances in Neural Information Processing Systems*, 34: 21834–21846.

Zhu, J.; Yan, Y.; Zhao, L.; Heimann, M.; Akoglu, L.; and Koutra, D. 2020. Beyond homophily in graph neural networks: Current limitations and effective designs. *Advances in Neural Information Processing Systems*, 33: 7793–7804.

Zhu, M.; Wang, X.; Shi, C.; Ji, H.; and Cui, P. 2021. Interpreting and Unifying Graph Neural Networks with An Optimization Framework. In *The Web Conference*, 1215–1226.

Appendix

Proof of Property 1

Z^* is order-invariant if we exchange the heterophilic and homophilic aggregation operations.

Proof.

$$\begin{aligned}
Z^* &= [(\alpha_1 I + h_1(L))(\alpha_2 I + h_2(L))]^{-1} X \\
&= (\alpha_2 I + h_2(L))^{-1}(\alpha_1 I + h_1(L))^{-1} X \\
&= U(\alpha_2 I + h_2(\Lambda))^{-1}(\alpha_1 I + h_1(\Lambda))^{-1} U^\top X \quad (19) \\
&= U(\alpha_1 I + h_1(\Lambda))^{-1}(\alpha_2 I + h_2(\Lambda))^{-1} U^\top X \\
&= [(\alpha_2 I + h_2(L))(\alpha_1 I + h_1(L))]^{-1} X.
\end{aligned}$$

□

Proof of Theorem 2

When $N \geq K$, $t \notin \{1, 2, \dots, K\}$, any N -order differentiable real-valued filter function can be approximated by N -order PC-Conv, with an error of order $N+1$.

Proof. Any N -order differentiable filter function $G(\lambda)$, $\lambda \in [0, 2]$, can be expanded by a N -order Taylor expansion, i.e., $G(\lambda) = \sum_{n=0}^N G^{(n)}(\lambda) \frac{\lambda^n}{n!} + O(\lambda^{N+1})$. The learning process of PC-filter $g_{k,t}(\lambda)$ via N -order Taylor expansion of $G(\lambda)$ can be expressed as:

$$\begin{aligned}
g_t(\lambda) &= \theta_0 + \sum_{k=1}^K \theta_k \cdot g_{k,t}(\lambda) = \theta_0 + \sum_{k=1}^K \theta_k \sum_{n=0}^N C_n(k, t) \frac{(-\lambda)^n}{n!} \\
&= \theta_0 + \sum_{n=0}^N \sum_{k=1}^K \theta_k C_n(k, t) \frac{(-\lambda)^n}{n!} = \sum_{n=0}^N G^{(n)}(\lambda) \frac{\lambda^n}{n!} \\
&\approx G(\lambda)
\end{aligned}$$

We have

$$\begin{cases} \sum_{k=1}^K \theta_k C_0(k, t) = G^{(0)}(\lambda) - \theta_0, n = 0 \\ \sum_{k=1}^K \theta_k C_n(k, t) = (-1)^n G^{(n)}(\lambda), n = 1, \dots, N \end{cases} \quad (20)$$

i.e.,

$$\begin{bmatrix} C_0(1, t) & C_0(2, t) & \dots & C_0(K, t) \\ C_1(1, t) & C_1(2, t) & \dots & C_1(K, t) \\ C_2(1, t) & C_2(2, t) & \dots & C_2(K, t) \\ \vdots & \vdots & \vdots & \vdots \\ C_N(1, t) & C_N(2, t) & \dots & C_N(K, t) \end{bmatrix} \begin{bmatrix} \theta_1 \\ \theta_2 \\ \vdots \\ \theta_K \end{bmatrix} = \begin{bmatrix} G^{(0)}(\lambda) - \theta_0 \\ -G^{(1)}(\lambda) \\ \vdots \\ (-1)^N G^{(N)}(\lambda) \end{bmatrix} \quad (21)$$

Denote the above equation as $A \cdot \theta = b$, $A \in R^{(N+1) \times K}$, $\theta \in R^K$, $b \in R^{N+1}$. We know that $G(\lambda)$ is arbitrary on different datasets or downstream tasks. Thus, the problem is equivalent to proving that there exists a set of coefficients $\{\theta_1, \dots, \theta_K\}$ that can make a linear combination of $A = \{A_{(1)}, \dots, A_{(K)}\}$ into arbitrary vector b . We only need to show that A is maximal linearly independent, i.e., the individual column vectors $\{A_{(1)}, \dots, A_{(K)}\}$ are linearly independent.

First, we assume that the individual column vectors $\{A_{(1)}, \dots, A_{(K)}\}$ are linearly correlated. Then there exists a set of coefficients that are not all zeros $\{\alpha_1, \dots, \alpha_K\}$, such that $\alpha_1 A_{(1)} + \dots + \alpha_K A_{(K)} = 0$.

$$\begin{aligned}
\alpha_1 C_0(1, t) + \dots + \alpha_K C_0(K, t) &= 0 \\
\alpha_1 C_1(1, t) + \dots + \alpha_K C_1(K, t) &= 0
\end{aligned}$$

⋮

$$\begin{aligned}
\alpha_1 C_{N-1}(1, t) + \dots + \alpha_K C_{N-1}(K, t) &= 0 \\
\alpha_1 C_N(1, t) + \dots + \alpha_K C_N(K, t) &= 0
\end{aligned}$$

i.e.,

$$\begin{bmatrix} \alpha_1 C_0(1, t) & \alpha_2 C_0(2, t) & \dots & \alpha_K C_0(K, t) \\ \alpha_1 C_1(1, t) & \alpha_2 C_1(2, t) & \dots & \alpha_K C_1(K, t) \\ \alpha_1 C_2(1, t) & \alpha_2 C_2(2, t) & \dots & \alpha_K C_2(K, t) \\ \vdots & \vdots & \vdots & \vdots \\ \alpha_1 C_N(1, t) & \alpha_2 C_N(2, t) & \dots & \alpha_K C_N(K, t) \end{bmatrix} \begin{bmatrix} 1 \\ 1 \\ 1 \\ \vdots \\ 1 \end{bmatrix} = \begin{bmatrix} 0 \\ 0 \\ 0 \\ \vdots \\ 0 \end{bmatrix} \quad (22)$$

Denote the above equation as $B \cdot \mathbf{1} = \mathbf{0}$, $B \in R^{(N+1) \times K}$, $\mathbf{1} \in R^K$, $\mathbf{0} \in R^{N+1}$. Second, define $\delta(x) = \max\{x, 0\}$ and $P_i \in R^{(N+1) \times (N+1)}$.

$$(P_i)_{mn} = \begin{cases} 1 & m = n = 1, \dots, N+1 \\ \delta(m-2-i)t & m = n-2, n \geq 3 \\ \delta(m-2-i) + t & m = n-2, n \geq 3 \\ 0 & \text{others} \end{cases} \quad (23)$$

Left multiplying both sides of Eq. (22) simultaneously by P_{N-1}, \dots, P_0 and employing the relation $C_{n+1}(\alpha, t) = (\alpha - n - t)C_n(\alpha, t) - ntC_{n-1}(\alpha, t)$, $n \geq 1$, we have

$$\begin{bmatrix} \alpha_1 C_0(1, t) & \alpha_2 C_0(2, t) & \dots & \alpha_K C_0(K, t) \\ \alpha_1 C_1(1, t) & \alpha_2 C_1(2, t) & \dots & \alpha_K C_1(K, t) \\ \alpha_1^2 C_1(1, t) & \alpha_2^2 C_1(2, t) & \dots & \alpha_K^2 C_1(K, t) \\ \vdots & \vdots & \vdots & \vdots \\ \alpha_1^N C_1(1, t) & \alpha_2^N C_1(2, t) & \dots & \alpha_K^N C_1(K, t) \end{bmatrix} \begin{bmatrix} 1 \\ 1 \\ 1 \\ \vdots \\ 1 \end{bmatrix} = \begin{bmatrix} 0 \\ 0 \\ 0 \\ \vdots \\ 0 \end{bmatrix} \quad (24)$$

With $t \notin \{1, 2, \dots, K\}$, it is guaranteed that $C_1(k, t) = k - t \neq 0$, $k \in \{1, \dots, K\}$. We have

$$\begin{bmatrix} \frac{C_0(1,t)}{C_1(1,t)} & \frac{C_0(2,t)}{C_1(2,t)} & \dots & \frac{C_0(K,t)}{C_1(K,t)} \\ 1 & 1 & \dots & 1 \\ \alpha_1 & \alpha_2 & \dots & \alpha_K \\ \vdots & \vdots & \vdots & \vdots \\ \alpha_1^N & \alpha_2^N & \dots & \alpha_K^N \end{bmatrix} \begin{bmatrix} \alpha_1 C_1(1, t) \\ \alpha_2 C_1(2, t) \\ \vdots \\ \alpha_K C_1(K, t) \end{bmatrix} = \begin{bmatrix} 0 \\ 0 \\ 0 \\ \vdots \\ 0 \end{bmatrix} \quad (25)$$

Third, we remove the first line and denote $F\theta^* = \mathbf{0}^*$, where

$$F = \begin{bmatrix} 1 & 1 & \dots & 1 \\ \alpha_1 & \alpha_2 & \dots & \alpha_K \\ \vdots & \vdots & \vdots & \vdots \\ \alpha_1^N & \alpha_2^N & \dots & \alpha_K^N \end{bmatrix}, \theta^* = \begin{bmatrix} \alpha_1 C_1(1, t) \\ \alpha_2 C_1(2, t) \\ \vdots \\ \alpha_K C_1(K, t) \end{bmatrix}, \mathbf{0}^* = \begin{bmatrix} 0 \\ 0 \\ \vdots \\ 0 \end{bmatrix}$$

Since the coefficient matrix F is a Vandermonde matrix, the solution θ^* is a zero solution. Because $C_1(i, t) \neq 0$,

$\{\alpha_1, \dots, \alpha_K\}$ are all zeros. Thus, it is a clear contradiction and the individual column vectors $\{A_{(1)}, \dots, A_{(K)}\}$ are linearly independent. \square

Experimental Settings

Dataset.

For the sake of fairness, we select benchmark datasets that are commonly used in related work. For the homophilic graph, we select three classic citation graphs: Cora, CiteSeer, PubMed (Yang, Cohen, and Salakhudinov 2016). For the heterophilic graph, we select four datasets including the Webpage graphs Texas, Cornell and Wisconsin from WebKB³, and the Actor co-occurrence graph (Pei et al. 2020). Besides, we also select Penn94 from Facebook 100⁴ as a representative dataset of the social network (Lim et al. 2021). We give the statistics for these datasets in Table 6, in which we use edge homophily ratio $h(G) = \frac{|\{(u,v):(u,v) \in \mathcal{E} \wedge y_u = y_v\}|}{|\mathcal{E}|}$ to measure the degree of homophily (Zhu et al. 2020).

Table 6: Dataset statistics.

Datasets	Cora	CiteSeer	Pubmed	Actor	Texas	Cornell	Wisconsin	Penn94
Nodes	2708	3327	19,717	7600	183	183	251	41,554
Edges	5278	4676	44,327	26,752	295	280	466	1,362,229
Features	1433	3703	500	931	1703	1703	5	
Classes	7	6	3	5	5	5	5	2
$h(G)$	0.81	0.74	0.80	0.22	0.11	0.30	0.21	0.47

Train/validation/test split.

For semi-supervised node classification in section 5.1, we split the dataset with random seeds according to (He, Wei, and Wen 2022). In detail, we select 20 nodes of each class on three homophilic datasets (Cora, CiteSeer, and Pubmed) for training, 500 nodes for validation, and 1000 nodes for testing. For the five heterophilic datasets, we apply the sparse splitting where the training/validation/test sets account for 2.5%/2.5%/95%.

For node classification, there are two common split ways: fixed seed splits and random seed splits. The former uses the fixed split given in (Li et al. 2022), which is commonly used in heterophilic GNNs. The latter, proposed by (Chien et al. 2021), uses random seeds for random split and is widely used in spectral GNNs, PDE GNNs, traditional methods, etc. To avoid unfair comparison, we evaluate the performance of PCNet under these two different settings. For the node classification with polynomial-based methods in section 5.2, we adopt 10 random seeds as (Chien et al. 2021; Wang and Zhang 2022) to randomly split the dataset into train/validation/test sets with a ratio of 60%/20%/20%. In section 5.3, we use the given split in (Li et al. 2022) to randomly split the dataset into training/validation/test sets at a ratio of 48%/32%/20%.

Training process.

We utilize Adam optimizer to optimize models and set the maximum number of iterations to 1000. In addition, we

³<http://www.cs.cmu.edu/afs/cs.cmu.edu/project/theo-11/www/wwkb>

⁴<https://archive.org/details/oxford-2005-facebook-matrix>

use the early stopping strategy to end training if the validation scores on the real-world dataset don't increase over time. For sections 5.1 and 5.2, we set the early-stop epoch threshold to 200, in line with (He, Wei, and Wen 2022; Wang and Zhang 2022; He et al. 2021). For section 5.3, we use the same settings as GloGNN++ (Li et al. 2022) and set the early-stop epoch threshold as a hyperparameter in the range {40, 200, 300}. For dataset Penn94, we use AdamW as the optimizer following (Li et al. 2022).

Computing infrastructure.

We leverage Pytorch Geometric and Pytorch for model development. All experiments are conducted on the same machine with the Intel(R) Core(TM) i7-8700 3.20GHz CPU, two GeForce GTX 1080 Ti GPUs and 64GB RAM. The implementation of PCNet will be public available upon acceptance.